# Group 1 and 2 suboxides and subnitrides — metals with atomic size holes and tunnels

Arndt Simon

*Max-Planck-Institut für Festkörperforschung, Stuttgart, Germany*

Received 7 November 1996; accepted 29 November 1996

## Contents

## Abstract

Alkali metal suboxides and the closely related subnitrides of alkaline earth metals represent a unique class of compounds. Their structures are composed of discrete clusters ($Rb_9O_2$, $Cs_{11}O_3$, $Ba_6N, Ba_{14}CaN_6$) which form stoichiometric compounds with alkali metals like $Rb_9O_2Rb_3 = Rb_6O$, $Cs_{11}O_3Cs_{10} = Cs_7O$, $Cs_{11}O_3Rb_7$, $Na_{16}Ba_6N$, or $Na_{22}Ba_{14}CaN_6$. In the structures of $NaBa_3N$ and $Na_5Ba_3N$ chains of condensed clusters are embedded in alkali metal. All compounds are metalic. Due to the cumulation of negative charges by $O^{2-}$ and $N^{3-}$ ions inside the clusters the conduction electrons reside in the space between the clusters. Electronic confinement in space leads to interesting physical properties. © 1997 Elsevier Science S.A.

## 1. Introduction

Metal–metal bonding is frequently found in compounds of metals in low oxidation state which results in discrete clusters or infinitely extending M–M bonded arrays. What is the expectation for metal-rich compounds of alkali and alkaline earth metals in terms of structures, bonding and properties? A comparison of special features of clusters within the general frame of the periodic table helps to answer the question qualitatively.

Metal cluster chemistry has been widely explored with d metals. Naturally, discrete clusters with the metal atom core surrounded by a ligand shell dominate solution chemistry. In the solid state such clusters may occur as discrete entities or linked *via* bridging ligands and even condensed by sharing metal atoms very much depending on the metal content in the compound [1,2]. Metal valence electron deficiency leads to the special feature that cluster structures are frequently stabilized by "interstitial" atoms. Thus, a part of the weak homonuclear M–M bonding is substituted by strong heteronuclear bonding within the cluster core. This feature is met with clusters of the valence–electron poor group 5 metals, becomes essential for group 4 metal clusters [3], and is the basis for a vast number of metal-rich halides of group 3 elements and lanthanides which were discovered in recent years [4]. It is interesting to note that M–M bonding and formation of discrete and condensed clusters with rare earth metals is frequently verified in the solid state, however still awaits discovery in solution chemistry. The situation is even more extreme with actinides. An extensive cluster chemistry of these elements can be predicted from both the behavior of the lanthanides as well as thorium [5,6]. This chemistry is clearly addressed but not yet opened.

The metals discussed so far offer a cluster chemistry that is gradually and systematically changing within the periodic table as a function of the available metal valence–electron concentrations [Fig. 1]. There is a characteristic stepwise sequence from strongly M–M bonded and ligand encapsulated clusters to clusters stabilized by interstitials and/or condensed cluster systems due to electron and ligand deficiency. This trend allows an extrapolation to the far left side of the periodic table. With group 1 and 2 metals one expects cluster systems which are stabilized by interstitials and have pronounced ligand deficiency. In fact, in alkali metal suboxides and alkaline earth metal subnitrides characteristic cluster systems occur which do not have any ligands at all.

These bare clusters and systems of condensed clusters interact *via* metallic bonding which results in a unique situation that is best illustrated by comparison with the characteristics of very large metal clusters. The latter, e.g. of gold or palladium [7,8], represent "nanoparticles" of a metal with delocalized electrons inside and an insulating ligand layer outside. An array of such clusters may be called "quantum-dot array" in analogy to much investigated semiconductor devices where the confinement of conduction electrons in space leads to quantization effects [9,10]. The situation is inverse with alkali metal suboxides and alkaline earth metal subnitrides.

The clusters of these electropositive metals contain the fixed negative charges of oxide and nitride anions inside which are repulsive to conduction electrons. These are therefore confined to the cluster periphery and the space between the clusters. Crystals of these compounds may be called "self-assembled anti-quantum-dot arrays" again in analogy to the corresponding semiconductor devices [9,10] and, as will be shown, the spatial confinement of conduction electrons again leads to quantum size effects.

The described bonding characteristics found for alkali metal suboxides were paralleled only recently with novel subnitrides, particularly involving barium. The following report spans a research period of twenty years.
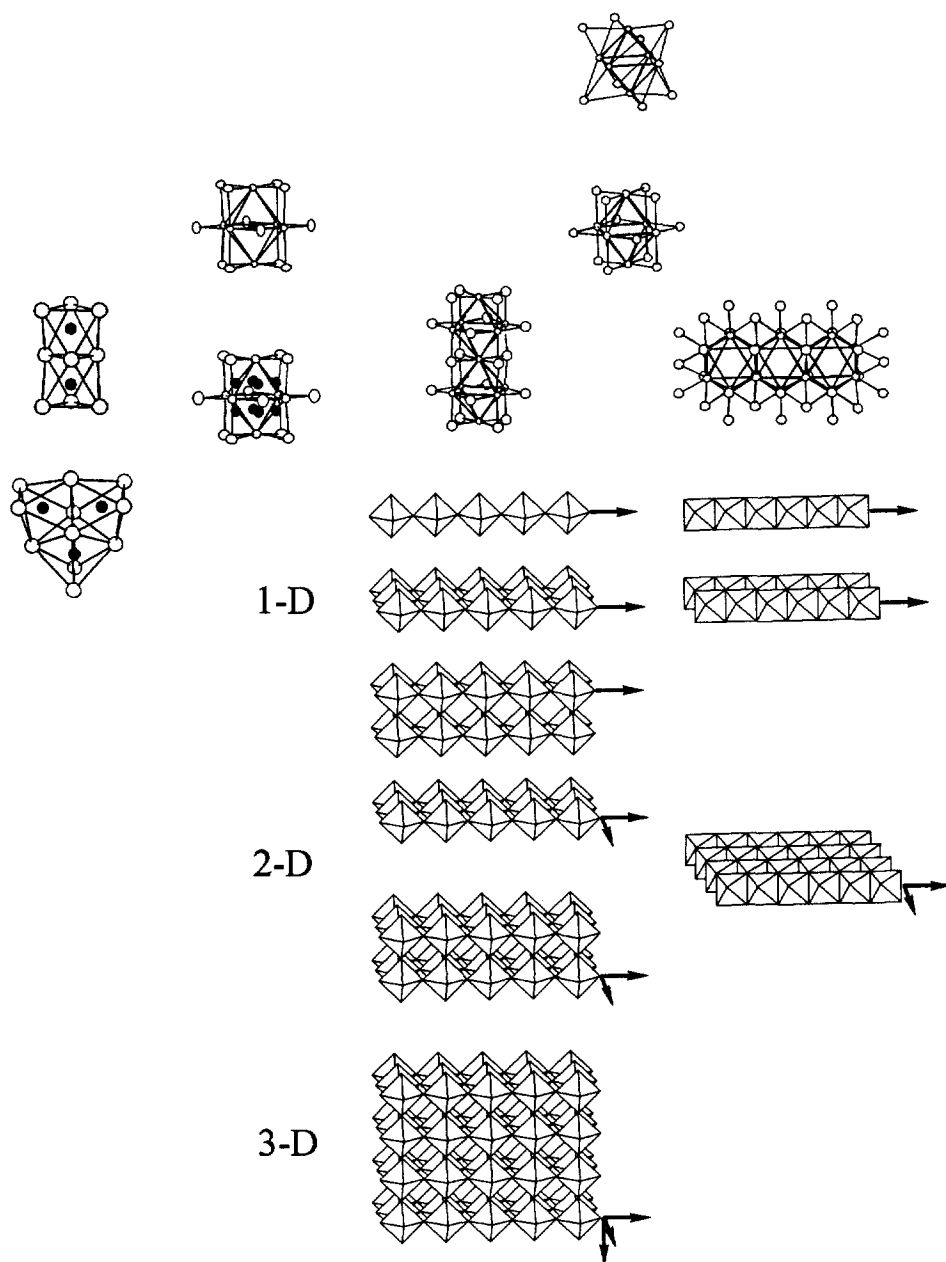
1-D

2-D

3-D

Fig. 1. $M_6X_8$ and $M_6X_{12}$ clusters which can occur discrete and condensed as shown for oligomeric and polymeric systems in oxoniobates (corner sharing) and oxomolybdates (edge sharing). In case of electron deficiency the clusters are stabilized by interstitial atoms, and such clusters occur condensed via edges in reduced phases of the rare earth metals. No ligand shell surrounds the clusters in alkali metal suboxides.

## 2. Alkali metal suboxides

When oxygen is very carefully added to a melt of cesium the native golden colour of the metal gradually darkens to bronze, violet and finally nearly black. Rubidium in the same reaction changes colour from that of silver to brass and finally copper. In both cases the oxygen is dissolved homogeneously in marked contrast to the lighter alkali metals which deposit the oxides $M_2O$ from their melts with an intermediate formation of dark surface layers and recovery of the silver colour of the pure metals.

From the coloured melts of oxidized rubidium and cesium, solid suboxides crystallize upon cooling as was shown first by Rengade around 1910 for cesium [11,12].

The findings of these admirable early investigations were verified with some corrections to the proposed formulae in our detailed investigations which also led to the characterization of the corresponding metal-rich oxides of rubidium as well as Rb–Cs mixed suboxides. The methods of preparation of the compounds and the characterization of their phase relationships, crystal structures, thermal, optical and electronic properties have been reported and reviewed comprehensively [13–17]. So, the facts will only be briefly summarized here with some mentioning of unsolved problems.

The chemistry of crystalline rubidium and cesium suboxides is a chemistry at temperatures between $-120°$ and $+150°C$. Mixed K–Cs suboxides also exist at low temperature, however decompose into $K_2O$ and K–Cs alloy at approximately $-60°C$. Those phases which have been fully characterized by thermal analysis and X-ray structure analysis are summarized in Table 1 [18–24]. Quite sophisticated investigations are needed as will be briefly illustrated for the example of rubidium suboxides.

Samples with appropriate, exactly known Rb–O content are easily prepared by reacting the distilled metal with oxygen liberated by thermally decomposing a weighed amount of HgO which has been prepared from the elements. The oxygen is quantitatively absorbed by rubidium in a vigorous reaction which must be carefully controlled to avoid evaporation of the metal. Thermal analyses of samples with

Table 1
Structurally characterized alkali metal suboxides; the number of formula units per cell, Z refers to the structural formula

| Compound | Structural Formula | Unit cell (at T) | Ref. |
|---|---|---|---|
| $Rb_9O_2$ | $Rb_9O_2$ | P $2_1/m$, Z=2, a=832.3, b=1398.6, c=1165.4 pm$\beta$=104.39° ($-50°C$) | [18] |
| $Rb_6O$ | $Rb_9O_2 \cdot Rb_3$ | P $6_3/m$, Z=2, a=839.3, c=3046.7 pm ($-50°C$) | [19] |
| $Cs_{11}O_3$ | $Cs_{11}O_3$ | P $2_1/c$, Z=4, a=1753.6, b=919.2, c=2401.7 pm$\beta$=100.42° ($-50°C$) | [20] |
| $Cs_4O$ | $Cs_{11}O_3 \cdot Cs$ | Pna2, Z=4, a=1682.3, b=2052.5, c=1237.2 pm ($-100°C$) | [21] |
| $Cs_7O$ | $Cs_{11}O_3 \cdot Cs_{10}$ | P-6 m 2, Z=1, a=1630.9, c=915.4 pm ($-50°C$) | [22] |
| $Cs_{11}O_3Rb$ | $Cs_{11}O_3Rb$ | Pmn2$_1$, Z=2, a=1646.4, b=1368.3, c=909.2 pm ($-80°C$) | [23] |
| $Cs_{11}O_3Rb_2$ | $Cs_{11}O_3Rb_2$ | P2$_1$, Z=8, a=4231.1, b=919.4, c=2415.6 pm ($-50°C$) | [14] |
| $Cs_{11}O_3Rb_7$ | $Cs_{11}O_3Rb_7$ | P2$_1$2$_1$2$_1$, Z=4, a=3228.1, b=2187.7, c=902.5 pm ($-90°C$) | [24] |

gradually increasing oxygen content reveal a seemingly simple eutectic system involving a suboxide which was first assigned the formula "Rb$_3$O" [25]. However, with high enough temperature resolution the effect due to "eutectic melting" splits into two very closely spaced effects, and the investigation with a specially designed X-ray camera [26] that allows a continuous observation with temperature changing by 0.3°C per day shows that actually two suboxides exist, the more metal-rich of both decomposing 0.3°C below the eutectic (Fig. 2).

Of course, an exact determination of phase compositions in such a complicated system is not possible *via* thermal and X-ray powder analysis alone. The problem was solved by *in situ* growth of single crystals on diffractometers using a miniaturized Bridgman technique [21] which, by the way, proved extremely helpful to grow crystals of low melting or decomposing molecular compounds from melt or solution such as N$_2$O$_3$ [27] or NOCl$_2$ [28] etc. The procedure allows to overcome equilibrium conditions kinetically. In the case of rubidium suboxides quenching of a sample RbO$_{0.126}$ to $-150°$ followed by slow warming leads to nutrients of the more oxygen-rich suboxide *via* amorphous and metastable crystalline phases [29], and quenching to only $-30°$C results in nutrients of the more metal-rich phase. Once specific nutrients are formed, suitable single crystals for the structure investigations of the compounds which turned out to be Rb$_6$O and Rb$_9$O$_2$, respectively, are grown using just one liquid sample RbO$_{0.126}$ filled into an X-ray capillary.

The known stable alkali metal suboxides exhibit a quite uniform structural chemistry. Basic units are Rb$_9$O$_2$ clusters formed from two face-sharing Rb$_6$O octahedra
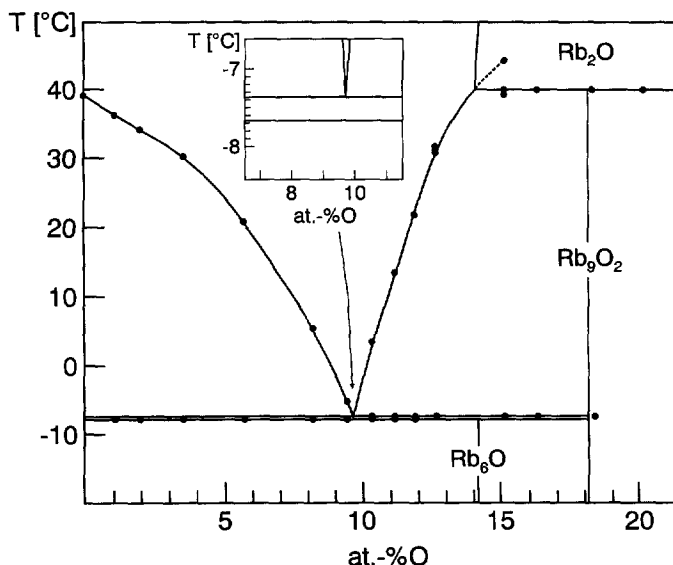


Fig. 2. Phase diagram of rubidium suboxides. Rb$_6$O decomposes into both solid Rb and Rb$_9$O$_2$ at a temperature which is 0.3°C below the eutectic melting temperature. Rb$_9$O$_2$ melts incongruently with the formation of "normal" Rb$_2$O.

in the case of rubidium suboxides and $Cs_{11}O_3$ clusters containing three face-sharing $Cs_6O$ octahedra in the case of cesium and Rb–Cs mixed suboxides, see Fig. 3. The difference of atomic size of Rb and Cs, respectively, is most probably the cause for the different cluster sizes.

These clusters are the only constituents of the compounds $Rb_9O_2$ and $Cs_{11}O_3$, respectively shown in Figs. 4a and 5a. The crystal structures of these two compounds give the impression of molecular crystals with short M–M distances within the clusters and large ones between them. However, when the inter- and intra-cluster distances are compared to those in the metals on one side and the normal oxides $M_2O$ on the other it becomes clear that the suboxide clusters are held together by strong heteropolar bonding, and the comparatively weak bonding between the clusters corresponds to that in the native metals. A more sophisticated treatise of bonding in terms of a spatial separation of ionic and metallic bonding shows that
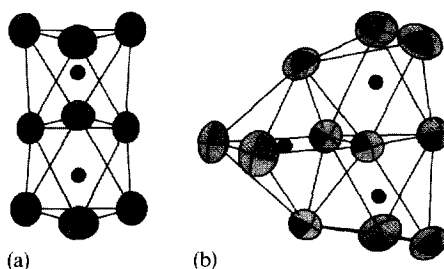


(a)                    (b)

Fig. 3. $Rb_9O_2$ (left) and $Cs_{11}O_3$ clusters in alkali metal suboxides (small spheres oxygen). The orientations of the large thermal ellipsoids indicate rigid M–O and soft M–M bonding.
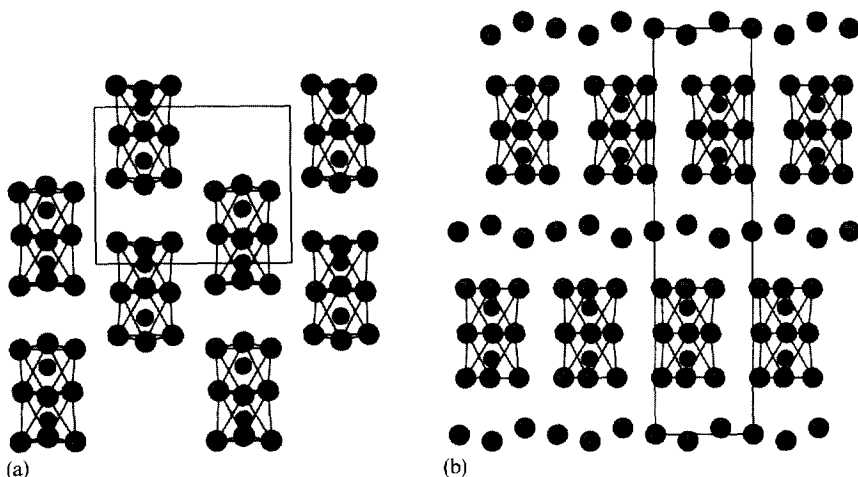


(a)                                      (b)

Fig. 4. Crystal structures of rubidium suboxides (a) $Rb_9O_2$ projected along the monoclinic a axis (b axis horizontal) and (b) $Rb_6O = Rb_9O_2 \cdot Rb_3$ projected on (110) of the hexagonal unit cell (c axis vertical), $Rb_9O_2$ clusters outlined.
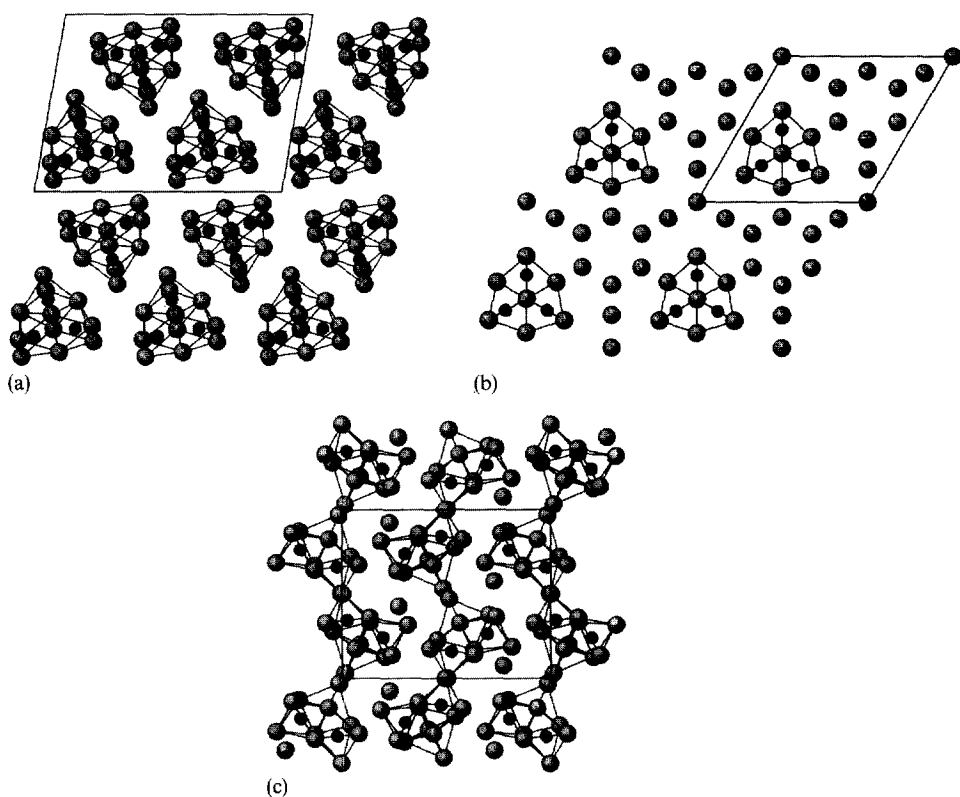
Fig. 5. Crystal structures of cesium suboxides (a) $Cs_{11}O_3$ projected along the monoclinic b axis (c axis horizontal), (b) $Cs_7O = Cs_{11}O_3 \cdot Cs_{10}$ projected along the hexagonal c axis and (c) $Cs_4O = Cs_{11}O_3 \cdot Cs$ projected along the orthorhombic c axis (b axis horizontal), $Cs_{11}O_3$ clusters outlined.

the M–M bonding is essential for the stability of these clusters [30]. The compounds $Rb_9O_2$ and $Cs_{11}O_3$ might be viewed as "complex metals", i.e. alkali metals where the single ion cores are substituted by ion complexes. A description as $(Rb^+)_9(O^{2-})_2 \cdot (e^-)_5$ and $(Cs^+)_{11}(O^{2-})_3 \cdot (e^-)_5$ seems reasonable in view of the extreme electronegativity difference of the heavy alkali metals compared to oxygen. Characteristic structural features such as a shift of the $O^{2-}$ ions out of the centers of the coordination octahedra towards the cluster periphery as a result of Coulomb repulsion are in favor of such a description. This simple view of bonding is corroborated quantitatively by specific heat [16], Raman [30], reflectivity [17] and photo electron spectroscopy [15] studies.

The outlined bonding scheme gives easy access to an understanding of the bonding in the more metal-rich suboxides, the structures of which are depicted in Figs. 4 and 5 together with those of $Rb_9O_2$ and $Cs_{11}O_3$.

These compounds represent strictly stoichiometric "intermetallic phases" between the above mentioned "complex metals" and additional alkali metal. To start with

the rubidium suboxides, the structure of $Rb_6O$ is composed of layers of Rb atoms corresponding to a formula $Rb_9O_2Rb_3$. The structure gives the impression of an atomic scale eutectic, the phase $Rb_9O_2$ and metallic Rb just starting to separate. One wonders whether the layer ratio needs to be fixed to 1:1. Additional layers of one or the other kind could easily be introduced into the close-packed arrangement. Indeed, there is some evidence for such (metastable?) phases to occur, as distinct though sporadic additional effects near the line of decomposition of $Rb_6O$ are observed in thermal analysis measurements.

In the presence of cesium the $Cs_{11}O_3$ type cluster is preferred. This can be embedded in a matrix of alkali metal as in the case of $Cs_{11}O_3 \cdot Cs_{10} = Cs_7O$ or simply alternate with single alkali metal atoms in the NiAs-type related arrangement of $Cs_{11}O_3 \cdot Cs = Cs_4O$. Rubidium and cesium which otherwise have an extremely similar chemistry can be easily separated in crystal space as shown in Fig. 6. Addition of oxygen to Rb–Cs alloys leads to the formation of $Cs_{11}O_3$ clusters with Rb taking the positions between the clusters, e.g. in $Cs_{11}O_3 \cdot Rb_7$, $Cs_{11}O_3 \cdot Rb_2$ and $Cs_{11}O_3 \cdot Rb$. Ranges of homogeneity exist which follow the general formula $Cs_{11}O_3(Rb,Cs)_x$. Only when the ratio O:Cs becomes larger than 3:11 some of the rubidium is incorporated into the cluster. Whereas this type of substitution has been studied in detail [31] the other type — Rb atoms in the $Rb_9O_2$ cluster being substituted by Cs atoms — needs to be further elucidated.

One more problem in alkali metal suboxide chemistry remains only partly understood. In the binary system an O:Cs ratio larger than 3:11 leads to the formation of yet another phase which has been described as $Cs_3O$. An early X-ray structure analysis made an assignment to the anti-$TiI_3$ type structure [32]. In a hexagonal close packed array of Cs atoms octahedral sites are occupied in such a way that straight chains of face sharing trigonal antiprisms $Cs_6O$ occur with again metallic bonding between them. Hence, the structural principle of condensing $M_6O$ octahedra *via* faces is still preserved, however, resulting in an infinite chain instead of a discrete
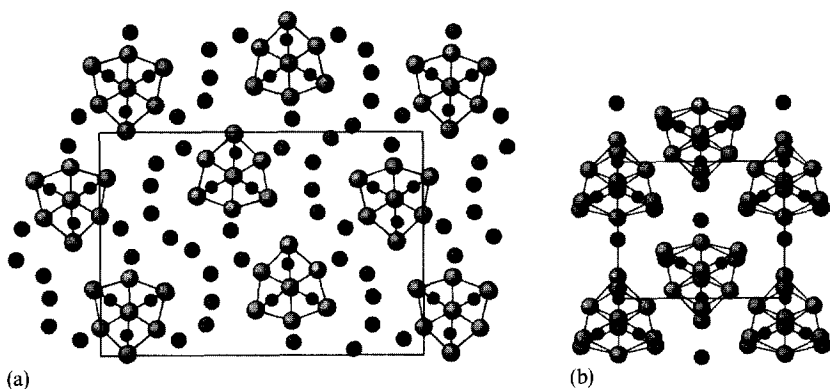


(a)                                                                 (b)

Fig. 6. Examples of Rb/Cs mixed suboxides. Structures of (a) $Cs_{11}O_3Rb_7$ projected along the orthorhombic c axis (b axis vertical) and (b) $Cs_{11}O_3Rb$ projected along the orthorhombic c axis (b axis vertical), $Cs_{11}O_3$ clusters outlined.

cluster. In spite of this principal consistency the structure of "Cs₃O" is puzzling. According to thermal analysis data, the phase has a large range of homogeneity which extends to both sides of the ideal composition $Cs_3O$ [13]. The most metal-rich phase is $Cs_{3.2}O$; the oxygen-rich limit has not been determined exactly but lies well below $Cs_{2.9}O$. Such deviation is easily understood for an oxygen atom deficiency but difficult to visualize for an excess of oxygen. Last but not least, experimental evidence is against the simple structural model. Strong diffuse scattering besides narrow Bragg reflections are characteristic for the X-ray pattern of a "Cs₃O" crystal. On the basis of the Bragg reflections the chain structure refines to $R = 0.04$, however, with ill-defined thermal parameters. Further work is needed in order to understand this structure, in particular as the $M_3X$ chain again occurs as an essential building unit in alkaline earth metal subnitrides.

## 3. Alkaline earth subnitrides

For a long time the structural principle seen with alkali metal suboxides seemed unique. Early attempts [33] to find similar bonding conditions with a combination of the neighboring elements, barium and nitrogen, revealed $Ba_2N$ which is isotypic with $Ca_2N$ [34] as the only subnitride. The reactions were performed with barium and nitrogen at temperatures near the melting point of the metal. Following the procedure of Addison et al. [35] we could recently approach a number of novel Na–Ba mixed subnitride phases. More are still to come.

The experimental techniques worked out for alkali metal suboxides, in-situ crystal growth on diffractometers in particular, proved essential for the characterization of the existing phases.

When reacting barium which is dissolved in liquid sodium with nitrogen at temperatures not too far away from the melting point of sodium, Addison et al. had observed the formation of barium-rich nitride clusters in the melt prior to the deposition of solid $Ba_2N$. Of course, the assumed compositions for the solution species had to be rather arbitrary. The isolation of solid subnitrides now gives direct access to the detailed characterization of such subnitride clusters. Those determined by single crystal structure investigations are summarized in Table 2 [36–41].

The most metal-rich compound to be formed is $Na_{16}Ba_6N$. It was crystallized from a melt of 20 mole-% barium in sodium which contained traces of nitrogen. The structure determined from a single crystal investigation is shown in Fig. 7. It is composed of discrete $Ba_6N$ octahedra regularly dispersed in an ordered array of metallic sodium. Again, as in the case of alkali metal suboxides the bonding is characterized by strong heteropolar bonds between N and Ba inside the $Ba_6N$ cluster, and metallic bonds between Ba and the Na atom matrix are clearly reflected in the interatomic distances. The $Ba_6N$ cluster itself relates to hypermetallated gas phase species like $Li_6C$ [42] which in our case are stabilized by insertion into a metallic environment. Obviously, the structural principle can be realized in quite different chemical systems. To give an example, the compound formerly described as the binary $Ag_8Ca_3$ [43] has to be reformulated as $Ag_{16}Ca_6N$, and it is isotypic

Table 2
Structurally characterized subnitrides involving barium

| Compound | Unit cell | Ref. |
|---|---|---|
| $Na_{16}Ba_6N$ | I m–3m, Z = 2, a = 1252.7 | [36] |
| $NaBa_3N$ | P $6_3$/mmc, Z = 2, a = 844.1, c = 698.2 pm | [37] |
| $Na_5Ba_3N$ | P nma, Z = 4, a = 1189.7, b = 705.6, c = 1780.1 pm | [38] |
| $Na_{14}Ba_{14}CaN_6$ | F m3m, Z = 8, a = 1789.5 pm | [39,40] |
| $Na_{17}Ba_{14}CaN_6$ | P − 1, Z = 2, a = 1114.2, b = 1206.5, c = 1372.5 pm $\alpha$ = 66.65, $\beta$ = 67.79, $\gamma$ = 78.88° | [40] |
| $Na_{21}Ba_{14}CaN_6$ | C 2/m, Z = 4, a = 2150.0, b = 1266.4, c = 1629.5 pm $\beta$ = 129.48° | [40] |
| $Na_{22}Ba_{14}CaN_6$ | P $6_3$/mmc, Z = 2, a = 1266.6, c = 1263.5 pm | [40,41] |
| $Ba_2N$ | R − 3m, Z = 3, (a = 403.1, c = 2253.2 pm) | [33] |
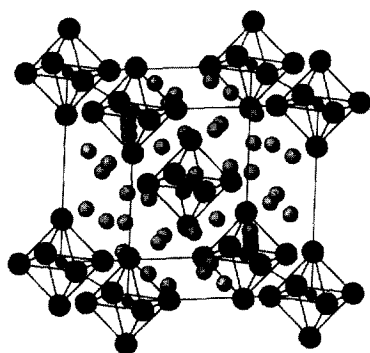


Fig. 7. Cubic unit cell of $Na_{16}Ba_6N$. The $Ba_6N$ octahedra are outlined.

with $Na_{16}Ba_6N$ [36] which might indicate the possible potential of an extension of subnitride chemistry.

The $M_6X$ cluster in $Na_{16}Ba_6N$ represents the basic unit, the single octahedron formed by the metal atoms and centered by a nonmetal atom, and this unit is used for the construction of larger units *via* condensation. Two such octahedra form the $M_9X_2$ cluster in rubidium suboxides and three of them the $M_{11}X_3$ cluster in cesium suboxides. The extreme of an infinite number of $M_6X$ units condensed into a chain as in "$Cs_3O$" also occurs with subnitrides and in this case in a well-defined way.

A compound containing such $Ba_3N$ chains, $NaBa_3N$, was identified as a major reaction product [37], when a Na–Ba alloy with approximate molar ratio 1:1 was reacted with a substoichiometric amount of nitrogen at 400°C and then cooled slowly to 100°C. Brittle black needles are easily isolated from the surface of the ductile metal regulus. In order to prepare the compound as a pure phase several different routes are possible: The reaction is performed with an excess of sodium and a stoichiometric amount of nitrogen. After cooling the product contains crystalline $NaBa_3N$ which is embedded in a matrix of sodium and the subnitride can be removed with an appropriate amount of potassium forming liquid K–Na alloy at

room temperature. Another way is to react the intermetallic compound NaBa [44] and the nitride $Ba_2N$ in an equimolar ratio at 150 to 250°C.

The structure of $NaBa_3N$ is shown in Fig. 8a. It contains parallel chains of composition $Ba_3N$, and as one would expect, the $Ba_6N$ units in the chain are deformed into elongated trigonal antiprisms due to Coulomb repulsion between the $N^{3-}$ ions. According to the formal description as $(Na^+)(Ba^{2+})_3N^{3-} \cdot (e^-)_4$ the excessive electrons provide M–M bonding in the chains, between Ba atoms themselves and between Na and Ba atoms. These electrons are delocalized in a conduction band with mixed Na–Ba character making the compound a metal as evidenced by photoelectron spectra and calculated band structure.

As in the case of alkali metal suboxides the extension of the purely metallic region between the ionic substructures can be varied. The pale-golden coloured compound $Na_5Ba_3N$ forms in the presence of an appropriate amount of sodium and is stable below 150°C. Its structure shown in Fig. 8b presents an only small variation of the building principle realized in $NaBa_3N$. The $Ba_3N$ chains are geometrically identical in both structures in spite of different site symmetries indicating that the sodium atom arrangement is the soft and easily adjustable constituent in the structure.

An interesting reaction occurs when $Na_5Ba_3N$ is treated with potassium at 100°C. Sodium is extracted from the compound, and liquid K–Na alloy forms besides solid $NaBa_3N$. Obviously, the lowered sodium activity in a K–Na alloy compared to a pure sodium melt determines the Na content of the solid subnitride. This observation is of importance for the preparation of discrete members of yet another series of subnitrides.

When K–Na alloys instead of pure Na as solvent were used the result was a great surprise [39]. Treating a prereacted heterogeneous sample of composition "$Ba_3N$" with liquid $K_{0.33}Na$ led to the formation of a few single crystals which could be isolated from the solution. The cubic structure was solved and refined to $R = 0.03$ as "$Na_{14}Ba_{14}KN_6$". In the structure clusters of composition "$Ba_{14}KN_6$" were



(a)                                    (b)                                    (c)
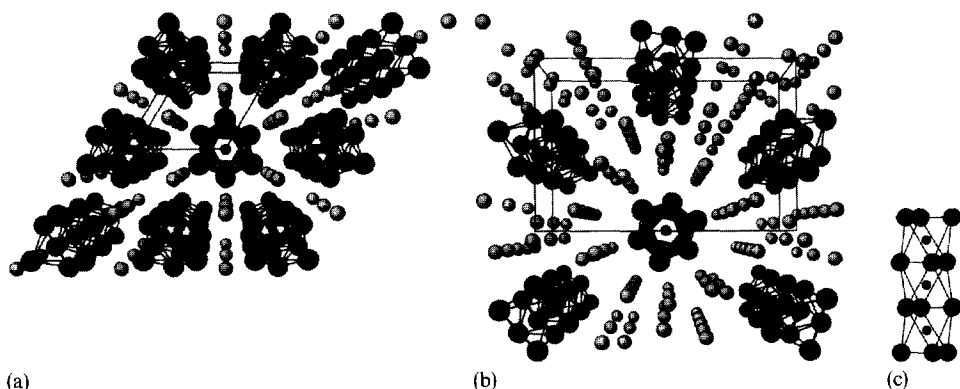
Fig. 8. Crystal structure of (a) $NaBa_3N$ projected along the hexagonal c axis and (b) $Na_5Ba_3N$ projected along the orthorhombic b axis (c axis horizontal). Both structures contain parallel $Ba_3N$ chains one of which is shown in a side view.

regularly dispersed in a sodium atom matrix. However, the coordination of the central $K^+$ ion by eight $N^{3-}$ ions seemed most unusual, and indeed, a systematic preparation of the compound failed. At the end, the central ion turned out to be $Ca^{2+}$. Obviously, calcium being present in 0.3 wt-% in the distilled barium underwent a highly selective incorporation into the cluster and led to the formation of crystals of $Na_{14}Ba_{14}CaN_6$. The compound is prepared in good yield when the necessary amount of calcium is purposely added. The nitrogen can also be introduced into the system as $N_2$ or *via* reaction with $Ba_2N$ or $NaN_3$. Clearly, the compound is a thermodynamically stable phase.

When reacted in the presence of a K–Na alloy of approximate composition $K_{0.5}Na$ the crystalline phases $Na_{14}Ba_{14}CaN_6$ and $Na_{17}Ba_{14}CaN_6$, respectively, could be isolated. In contrast, the use of pure sodium as a solvent led to the crystallization of $Na_{21}Ba_{14}CaN_6$ and $Na_{22}Ba_{14}CaN_6$, respectively. Experimental details are given in [40,41].

All structures contain the $Ba_{14}CaN_6$ cluster shown in Fig. 9 with only marginal differences in geometrical details. This cluster occurs in different kinds of a Na atom matrix. The crystal structures of $Na_xBa_{14}CaN_6$ ($x = 14$, 17, 21, 22) are presented in Fig. 10.

The $Ba_{14}CaN_6$ cluster is built from a central Ca atom surrounded by an octahedron of N atoms and by a cube and finally an octahedron of Ba atoms. Another description is in line with that for alkali metal suboxides. Instead of only two and three $M_6X$ octahedra in the suboxide clusters, six such octahedra are condensed *via* faces with one common apex atom in the case of the new subnitride cluster. This cluster is formed with both Ca as well as Sr as the central atom but not Ba which seems to be too large. The phases $Na_xBa_{14}CaN_6$ are stoichiometric compounds. A partial substitution of the Na by K atoms does not occur, neither is there an indication for Na atom vacancies.

The unusual bonding situation described for the alkali metal suboxides in terms of clusters with strong ionic bonds inside being dispersed in a metallic matrix becomes particularly obvious with the compounds $Na_xBa_{14}CaN_6$. The formula can
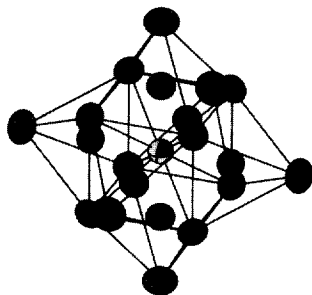


Fig. 9. $Ba_{14}CaN_6$ cluster composed of six face sharing $CaBa_5N$ octahedra with a common Ca atom. The cluster contains a central Ca atom surrounded by a cube and an octahedron of Ba atoms with six N atoms slightly above the cube faces.
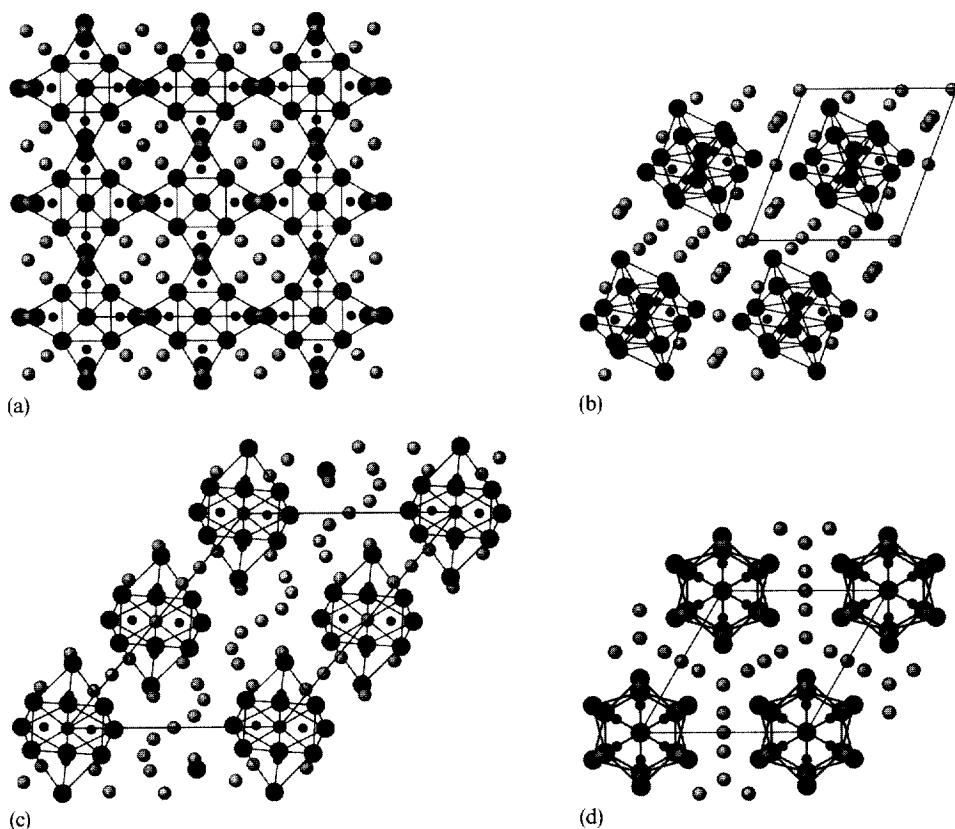
Fig. 10. Crystal structures of (a) cubic $Na_{14}Ba_{14}CaN_6$ projected along a cell edge, (b) $Na_{17}Ba_{14}CaN_6$ projected along the triclinic c axis (b axis horizontal), (c) $Na_{21}Ba_{14}CaN_6$ projected along the monoclinic b axis (c axis horizontal) and (d) $Na_{22}Ba_{14}CaN_6$ projected along the hexagonal c axis. The $Ba_{14}CaN_6$ clusters are outlined.

be decomposed into an intermetallic part $Na_xBa_6$ and an electroneutral salt-like part $Ba_8CaN_6$. The cube of large M atoms centered by a small M' atom with nonmetal atoms approximately in the centers of each face corresponds to a fragment of the (anti-)perovskite type structure [39] which is shown in its usual unit cell representation in Fig. 11 together with the cell shifted by $\frac{1}{2} \frac{1}{2} \frac{1}{2}$.

The arrangement of such atomic-scale particles $(Ba^{2+})_8Ca^{2+}(N^{3-})_6$ in the $Na_xBa_6$ matrix can be described as a nanoscopic dispersion of a salt in a metal which is depicted for the special representative $Na_{14}Ba_{14}CaN_6$ in Fig. 12.

## 4. Structure property relations

The structure of $Na_{14}Ba_{14}CaN_6$ as visualized in Fig. 12 shows the compound as a very special kind of metal. As would be the case with a microscopic dispersion of
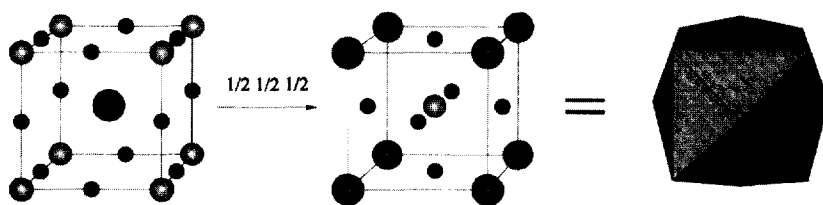
Fig. 11. Unit cell of a hypothetical anti-perovskite type $BaCaN_3$ together with the same cell shifted by $\frac{1}{2}\frac{1}{2}\frac{1}{2}$. N, Ca and Ba drawn with an increasing size.
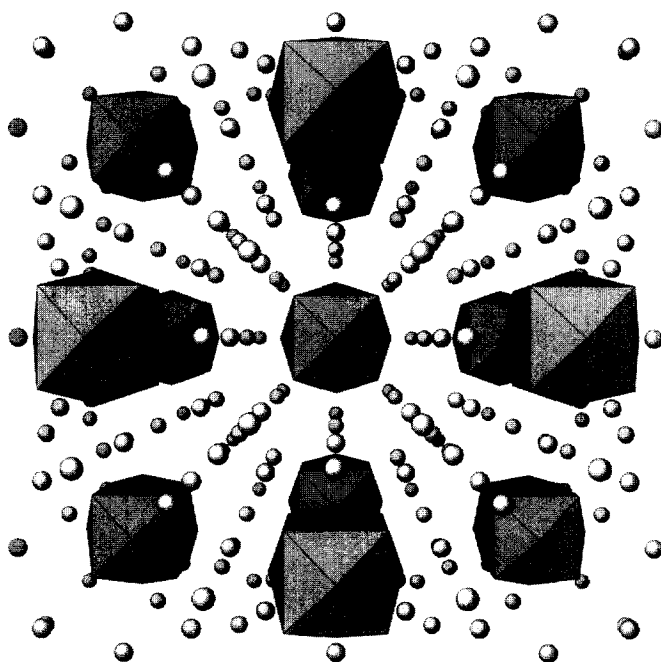


Fig. 12. Representation of the structure of $Na_{14}Ba_{14}CaN_6$ as a nanoscopic suspension of salt-like $Ba_8CaN_6$ "particles" in a metallic $Na_{14}Ba_6$ matrix.

salt particles in a metal, the conduction electrons are confined to the metallic part of the structure. The clusters with their large accummulation of negative charges are repulsive to the conduction electrons and hence act like voids which form a regular array in the metal. A peculiar property of such a "void metal" has been addressed earlier with alkali metal suboxides.

In Fig. 13 photoelectron spectra [15] of cesium and its suboxides are compared. All specific features in the spectra could be assigned such as the density of states at the Fermi level $E_F$ indicating metallic properties, the very narrow O2p band at only 2.7 eV binding energy indicative of a weakly stabilized oxygen dianion, the Cs5p band region with its characteristic multiple structure which allows distinction
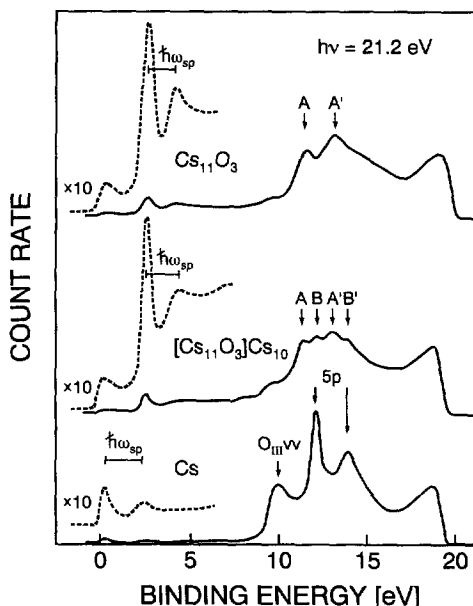
Fig. 13. Photoelectron spectra (UPS) of Cs, $Cs_7O$ and $Cs_{11}O_3$, He I excitation.

between the Cs atoms in purely metallic bonding and those forming the clusters. In addition, Auger peaks ($O_{111}VV$) and energy loss structures due ($\hbar\omega sp$) to surface plasmon excitations occur. The analysis of the energy loss structures allows a determination of the number of conduction electrons and hence puts the formal description of e.g. $Cs_{11}O_3$ as $(Cs^+)_{11}(O^{2-})_3 \cdot (e^-)_5$ on safe quantitative grounds. The corresponding UPS investigations of the subnitride phases are still in a rather preliminary state, however, the characteristic features at and near Fermi level give evidence for the metallic nature of the compounds as well as the presence of $N^{3-}$ ions which are only weakly stabilized by the Coulomb field of the surrounding cations in close analogy to the $O^{2-}$ ions in suboxides.

The spectra in Fig. 13 reveal one more characteristic feature not yet mentioned. The gap between the excitation energy 21.2 eV and the threshold of photo electrons becomes smaller upon oxidation of cesium. The gap represents the excess kinetic energy which is needed for the electrons to escape into vacuum and, hence, is a direct measure of the work function. As can be seen, the work function of cesium, $\phi \approx 2$ eV, which is the lowest of all elements is further decreased by approximately 0.6 eV when the compound $Cs_{11}O_3$ is formed.

A decrease of the work function upon oxidation of Rb and Cs is also found from wetting experiments with liquid helium [45,46] which show that partially oxidized rubidium exhibits wetting properties close to those of cesium.
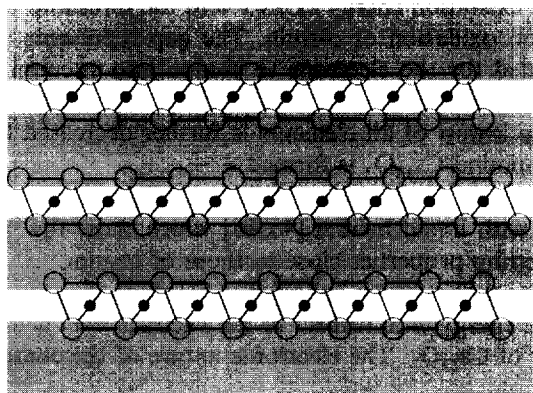
Model calculations for the cesium suboxides [47] show that the decrease of $\phi$, i.e. the increase of Fermi energy with respect to the vacuum level is due to the unusual void metal character of $Cs_{11}O_3$. The electronic nature of the compound is depicted
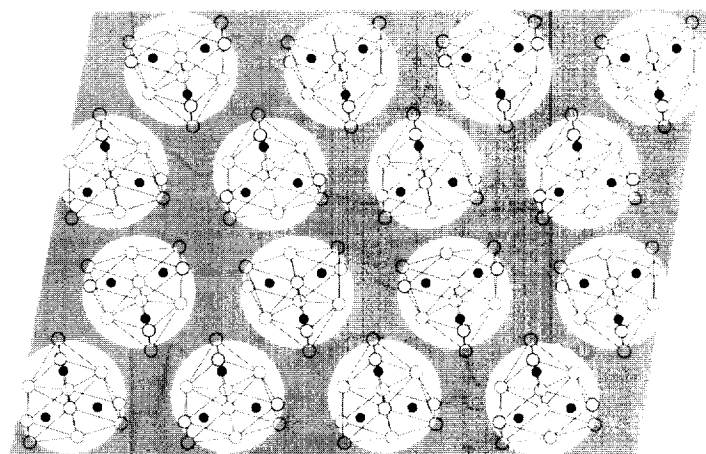
(a)
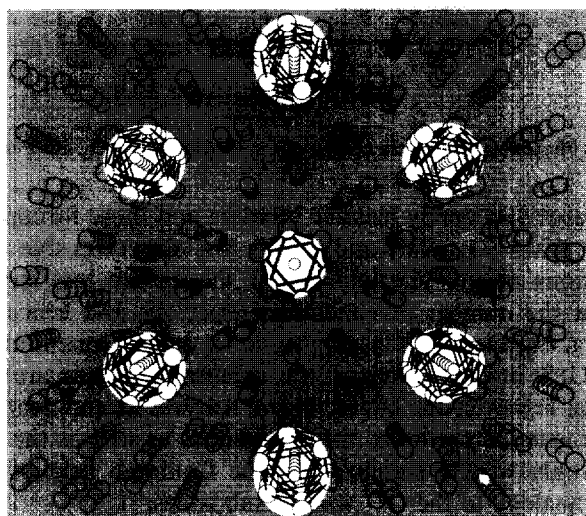


(b)



(c)

Fig. 14. Visualization of the real space electronic nature of selected suboxides and subnitrides. The shaded asreas indicate the regions of confinement of the conduction electrons. (a) $Cs_{11}O_3$ shown as a void metal, (b) $Na_5Ba_3N$ representing an atomically drilled metal and (c) $Ba_2N$ shown as a 2D-metal.

in Fig. 14a. Due to the charge 6- from the three $O^{2-}$ ions inside each cluster electrostatic repulsion leads to a confinement of the electron gas to the intercluster region, and the increase of the Fermi energy is due to a quantum size effect.

It should be mentioned that this fundamental property of a void metal finds an interesting application [48]. Infra-red sensitive photocathodes, e.g. in image converters (night vision devices) have been produced for many years which utilize layer-wise deposited Cs and $Cs_2O$ on a transparent silver substrate as an electron emitter. The low-energy photoemission had been explained on the basis of physical models, i.e. heterojunction models involving Cs and $Cs_2O$ layers. However, it could be demonstrated by UPS investigations of in-situ prepared photocathodes that suboxide formation is the source of this effect [49].

Having in mind that the ion clusters in alkali metal suboxides and alkaline earths subnitrides act as repulsive Coulomb bubbles to conduction electrons it is tempting to think about the consequence of special infinite arrays of $N^{3-}$ ions in such electropositive metals. The compounds $NaBa_3N$ and $Na_5Ba_3N$ contain parallel rows of anions in a metallic matrix. They represent realizations of what may be called "atomically drilled" metals visualized in Fig. 14b, and they are the first examples of an antitype to the well known and much investigated class of one-dimensional metals. Last, but not least, the structural principle of $Ba_2N$ (Fig. 14c) adds a new variant to the large class of two-dimensional metals.

It is fascinating to see the "colorless chemistry" of group 1 and 2 elements in their normal oxidation states to change into an in every respect colorful chemistry with metal-rich compounds. These materials organize themselves into most remarkable mesoscalic structures, to use the terms of our time.

# References

[1] A. Simon, Angew. Chem. Int. Ed. Engl. 27 (1988) 159.

[2] A. Simon, Clusters and Colloids, from Theory to Application, in: G. Schmid (Ed.), VCh Weinheim, New York, Basel, Cambridge, Tokyo, 1994, pp. 373.

[3] R.P. Ziebarth, J.D. Corbett, Acc. Chem. Res. 22 (1989) 256.

[4] A. Simon, Hj. Mattausch, G.J. Miller, W. Bauhofer, R.K. Kremer, in: K.A. Gschneidner jr., L. Eyring (Eds.), Handbook on the Physics and Chemistry of Rare Earths, Vol. 15, North Holland Publ., Amsterdam, London, New York, Tokyo, (1991), pp. 191.

[5] T.P. Braun, A. Simon, F. Ueno, F. Böttcher, Eur. J. Solid State Inorg. Chem. 33 (1996) 251.

[6] T.P. Braun, M. Mehring, A. Simon, J. Am. Chem. Soc. 118 (1996) 7203.

[7] G. Schmid, Clusters and Colloids, from Theory to Application, in: G. Schmid (Ed.), Vch Weinheim, New York, Basel, Cambridge, Tokyo, 1994, pp. 178.

[8] M.N. Vargastik, V.P. Zagorodnikov, I.P. Stolyarov, I.I. Moiseev, V.A. Likholobov, D.I. Kochubcy, A.L. Chuvilin, V.I. Zaikovsky, K.I. Zamaraev, G.I. Timofeeva, J. Chem. Soc., Chem. Commun. (1985) 937.

[9] T. Fulton, G. Dolan, Phys. Rev. Lett. 80 (1987) 72.

[10] Quantum dynamics of Submicron Structures, in: H.A. Cerdeira, B. Kramer, G. Schön (Eds.), NATO ASI Series E: Appl. Sciences Vol. 291 Kluwer Acad. Publ., Dordrecht, Boston, London (1995)

[11] E. Rengade, Bull. Soc. Chim. France, [4] 5 (1909) 994.

[12] E. Rengade, C.R. Acad. Sci. Paris 148 (1909) 1199.

[13] A. Simon, Z. anorg. allg. Chem. 395 (1973) 301.

[14] A. Simon, Structure and Bonding 36 (1979) 81.

[15] G. Ebbinghaus, A. Simon, J. Chem. Phys. 43 (1979) 117.

[16] E. Gmelin, A. Simon, W. Brämer, R. Villar, J. Chem. Phys. 76 (1982) 6256.

[17] G. Metsch, W. Bauhofer, A. Simon, Z. Naturforsch. 40a (1985) 303.

[18] A. Simon, Z. anorg. allg. Chem. 431 (1977) 5.

[19] A. Simon, H.-J. Deiseroth, Rev. Chim. Minér. 13 (1976) 98.

[20] A. Simon, E. Westerbeck, Z. anorg. allg. Chem. 428 (1977) 187.

[21] A. Simon, H.-J. Deiseroth, E. Westerbeck, B. Hillenkötter, Z. anorg. allg. Chem. 423 (1976) 203.

[22] A. Simon, Z. anorg. allg. Chem. 422 (1976) 208.

[23] H.-J. Deiseroth, A. Simon, Z. anorg. allg. Chem. 463 (1980) 14.

[24] A. Simon, W. Brämer, H.-J. Deiseroth, Inorg. Chem. 17 (1978) 875.

[25] P. Touzain, M. Caillet, Rev. Chim. Minér. 8 (1971) 277.

[26] A. Simon, J. Appl. Crystallogr. 4 (1971) 138.

[27] J. Horakh, H. Borrmann, A. Simon, Chem. Europ. J. 1 (1995) 389.

[28] A. Obermeyer, H. Borrmann, A. Simon, J. Am. Chem. Soc. 117 (1995) 7887.

[29] H.-J. Deiseroth, A. Simon, Z. Naturforsch. 33b (1978) 714.

[30] T.P. Martin, H.-J. Stolz, G. Ebbinghaus, A. Simon, J. Chem. Phys. 70 (1979) 1096.

[31] H.-J. Deiseroth, A. Simon, Rev. Chim. Minér. 20 (1983) 475.

[32] K.-R. Tsai, P.M. Harris, E.N. Lassettre, J. Phys. Chem. 60 (1956) 345.

[33] T. Künzel, Thesis, Stuttgart (1980).

[34] E.T. Keve, A.C. Skapski, Inorg. Chem. 7 (1968) 1757.

[35] C.C. Addison, R.J. Pulhaus, E.A. Trevillion, J. Chem. Soc. 20 (1975) 2082.

[36] G.J. Snyder, A. Simon, Angew. Chem. Int. Ed. Engl. 33 (1994) 689.

[37] P.E. Rauch, A. Simon, Angew. Chem. Int. Ed. Engl. 31 (1992) 1519.

[38] G.J. Snyder, A. Simon, J. Am. Chem. Soc. 117 (1995) 1996.

[39] U. Steinbrenner, A. Simon, Angew. Chem. Int. Ed. Engl. 35 (1996) 552.

[40] A. Simon, U. Steinbrenner, J. Chem. Soc. Faraday Trans. 92 (1996) 2117.

[41] U. Steinbrenner, A. Simon, Z. Kristallogr., 212 (1997) 428.

[42] P.v.R. Schleyer, E.-U. Würthwein, J.A. Pople, J. Am. Chem. Soc. 104 (1982) 5839.

[43] L.D. Calvert, C. Rand, Acta Crystallogr. 17 (1964) 1175.

[44] G.J. Snyder, A. Simon, J. Chem. Soc. Dalton Trans. (1994) 1159.

[45] J. Dupont-Roc, G. Misguich, L. Girlanda, Czech. J. Phys. 46 (S1) (1996) 419.

[46] B. Demolder, J. Dupont-Roc, J. Low Temp. Phys. 104 (1996) 1.

[47] M.G. Burt, V. Heine, J. Phys. C 11 (1978) 961.

[48] A.H. Sommer, Photoemissive Materials, Wiley, New York (1968), p. 163.

[49] G. Ebbinghaus, W. Braun, A. Simon, K. Berresheim, Phys. Rev. Lett. 37 (1976) 1770.